Evidence from meimechites and other low-degree mantle melts for redox controls on mantle-crust fractionation of platinum-group elements

James E. Mungall*†, Jacob J. Hanley*‡, Nicholas T. Arndt§, and Anne Debecdelievre§

*Department of Geology, University of Toronto, 22 Russell Street, Toronto, ON, Canada M5S 3B1; and §University Joseph Fourier, 1381 Rue de la Piscine, 38401 Grenoble, France

Edited by Stanley R. Hart, Woods Hole Oceanographic Institution, Woods Hole, MA, and approved June 28, 2006 (received for review February 2, 2006)

Understanding of the geochemistry of the chalcophile elements [i.e., Os, Ir, Ru, Pt, Pd (platinum-group elements), and Au, Cu, Ni] has been informed for at least 20 years by the common assumption that when crust-forming partial melts are extracted from the upper mantle, sulfide liquid in the restite sequesters chalcophile elements until the extent of partial melting exceeds ≈25% and all of the sulfide has been dissolved in silicate melt [Hamlyn, P. R. & Keays, R. R. (1985) *Geochim. Cosmochim. Acta* 49, 1797–1811]. Here we document very high, unfractionated, chalcophile element concentrations in small-degree partial melts from the mantle that cannot be reconciled with the canonical residual sulfide assumption. We show that the observed high, unfractionated platinum-group element concentrations in small-degree partial melts can be attained if the melting takes place at moderately high oxygen fugacity, which will reduce the amount of sulfide due to the formation of sulfate and will also destabilize residual monosulfide solid solution by driving sulfide melts into the spinel-liquid divariant field. Magmas formed at high oxygen fugacity by small degrees of mantle melting can be important agents for the transfer of chalcophile elements from the upper mantle to the crust and may be progenitors of significant ore deposits of Pt, Pd, and Au.

gold | oxidation | sulfide

The convecting part of the upper mantle is commonly thought to contain 250 ppm S as Fe–S–O (sulfide) liquid at the solidus temperature and oxidation state of sublithospheric peridotite (1, 2), although S concentrations between 50 and 300 ppm have been determined in xenoliths of variably melt-depleted and metasomatized subcontinental lithosphere (3). Sulfide/silicate partition coefficients range from ≈1,000 for the base metals Cu and Ni to >10,000 for platinum-group elements (PGE) and Au (4), causing sequestration of these chalcophile elements in sulfide liquid in the upper mantle residual to partial melting as long as sulfide is present. Because basalt dissolves ≈1,000 ppm of sulfide (5), sulfide melt will not persist after ≈25% of the mantle has melted if it initially contained 250 ppm S. Once sulfide is consumed, distribution of chalcophile elements depends only on their partitioning behavior between melt and solid restite.

Komatiites have high, unfractionated, chalcophile element concentrations compared with bulk silicate Earth (7) (Fig. 1). Their compositions can be modeled by assuming >25% partial melting of primitive mantle. Mid-ocean ridge basalts (MORB), which form by 10–15% melting, are strongly depleted in chalcophile elements (2, 7), consistent with the assumption that the PGE were retained in a sulfide phase that remained in the restite. However, the retention of sulfide liquid in the restite should produce a flat, unfractionated PGE signature that is very different from what is observed. Furthermore, ocean island basalts (OIB) show relatively high concentrations of the chalcophile elements, despite their origins through very low degrees of partial melting (7).

The reigning assumption of sulfide retention in the sources of low-degree partial melts of the mantle is inconsistent with their observed compositions. Bockrath *et al.* (8) recently addressed this issue, proposing that ascending silicate magmas entrain residual sulfide liquid while leaving residual monosulfide solid solution (mss) trapped in the residue. We have argued that this proposal is impossible because of the difficulty of forcing sulfide liquid droplets through pore throats in partially molten peridotite at low melt fractions (9) and seek instead an explanation based solely on sulfide phase relations during mantle melting. One geochemical factor that might affect the stability of sulfide liquid is the oxidation of sulfide to form sulfate (10); another is the solidification of sulfide liquid at high pressure to form an mss (8).

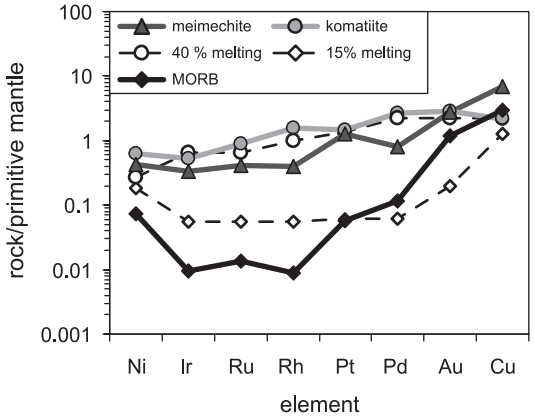

Fig. 1. PGE concentrations in samples of meimechite, komatiite, and MORB. Pyrolite (6) equilibrium melting models are shown for comparison (see *Discussion* for explanation).

We have determined the redox state and the concentrations of chalcophile elements in a suite of meimechites and alkali picrites, which are among the most extreme examples of low-degree asthenospheric partial melts known. We show that the canonical treatment of chalcophile element distribution during mantle melting must be revisited to account for the effects of redox controls on the phase relations of sulfide in the upper mantle.

Samples

Description. Meimechites are picritic magmas characterized by MgO contents >18 wt%, Na_2O+K_2O <1 wt%, and TiO_2 contents >1 wt% (11). Our suite of comagmatic samples includes examples

Conflict of interest statement: No conflicts declared.

This paper was submitted directly (Track II) to the PNAS office.

Abbreviations: PGE, platinum-group elements; MORB, mid-ocean ridge basalts; OIB, ocean island basalts; FMQ, fayalite–magnetite–quartz oxygen buffer; mss, monosulfide solid solution; ICP-MS, inductively coupled plasma MS; IPGE, iridium-group PGE; PPGE, plantinum-group PGE; fO_2, oxygen fugacity; fS_2, sulfur fugacity.

†To whom correspondence should be addressed. E-mail: mungall@geology.utoronto.ca.

‡Present address: Eidgenössische Technische Hochschule Zürich, Departement Erdwissenschaften, Clausiusstrasse 25, 8092 Zürich, Switzerland.

with Na_2O+K_2O both greater than and less than one, thus encompassing a series from meimechite to alkali picrite. The samples described here are previously undescribed samples from a Permian lava suite previously described from the Meimecha–Kotui region of northern Siberia (12, 13). With one aphyric exception, the rocks are strongly olivine-phyric, containing up to 30% of olivine crystals in a fine-grained groundmass with a partially devitrified intersertal texture. We consider the presence of deformation textures and trails of secondary melt inclusions in most included olivine crystals to be evidence that these rocks are xenocrysts whose euhedral margins reflect late overgrowth during ascent and decompression of the magma. Most olivine crystals also include crystals of chromite, some of which remain in contact with the interstitial glass, whereas others are wholly surrounded by their host olivine. We take this textural relation to indicate that both the mantle source region and the magma as it erupted were cosaturated in olivine and chromite. The intersertal texture of the groundmass is defined by diabasic-textured plagioclase, clinopyroxene, phlogopite, spinel, and olivine suspended in a matrix of isotropic brown glass. The samples have been weakly affected by low-temperature alteration, which caused widespread devitrification of the glassy groundmass and minor incipient serpentinization of olivine.

Compositions of Meimechite and Alkali Picrite. All lithogeochemical analyses were performed at the Geoscience Laboratory of the Ontario Geological Survey (Sudbury, ON, Canada). PGE concentrations were determined by NiS fire assay of 50-g aliquots of powdered rock samples, followed by acid digestion of the bead, Te coprecipitation, and inductively coupled plasma (ICP)-MS finish (14). Major elements were analyzed by wavelength dispersive x-ray fluorescence (WXRF) on glass beads; some trace elements were analyzed by WXRF on pressed powder pellets; other trace elements were determined by acid digestion in closed Teflon beakers followed by ICP-MS. Detection limits and analytical results for eight samples of meimechite and alkali picrite are listed in Table 1. Replicate analyses of PGE in international certified reference materials TDB-1, UMT-1, WGB-1, and WPR-1 performed between August 2004 and March 2005 are listed in Table 2, which is published as supporting information on the PNAS web site. Our results for UMT-1 differ from old certified values but are in excellent agreement with more recent determinations by isotope dilution–ICP-MS (15).

The samples form a continuum from meimechite to alkali picrite. One sample, 2-FG50, is aphyric in one half but crystal-rich in the other. The aphyric portion, which is most likely to retain the composition of a chilled liquid, is an alkali picrite containing 19.42 wt% MgO. The higher MgO and lower alkali contents of the remaining samples, including the crystal-rich half of the aphyric sample, allow classification of most as meimechite, largely because of the diluting effects of olivine xenocrysts. The composition of the aphyric portion of 2-FG50 is plotted in Fig. 1 for comparison with the composition of a typical komatiite magma and the predictions of models of 30% and 15% partial melting of upper mantle, assuming that the upper mantle contains 250 ppm S in the form of sulfide liquid. The high levels of PGE in the alkali picrite, similar to those of komatiite, and its correspondence to the 30% melting model, suggest that little, if any, sulfide liquid remained in the mantle restite.

The lack of a residual sulfide signature in the alkali picrite is sharply at odds with the inference from lithophile element concentrations that these magmas resulted from ≈1% partial melting, or 7% at most if a mantle source enriched in incompatible elements is invoked (12). It is especially problematic in light of the fact that sulfide solubility in basaltic melts decreases with increasing pressure (5). Subcratonic garnet peridotites residual to 30% melting at great depth can contain residual sulfide (16), whereas some abyssal harzburgites that have undergone 12–15% low-pressure melting retain no sulfide whatsoever (17). These contrasting observations indicate that deep-seated magmas such as meimechites should be even less able to dissolve sulfide than MORB, making the lack of residual sulfide signature in these low-degree melts even more surprising. A resolution of this paradox must be sought in other factors that influence the stability of sulfide liquid in the mantle source, including oxidation state and the possible role of mss crystallization.

Mineral Compositions. We have estimated the temperature and oxygen fugacity (fO_2) of equilibration of 27 adjacent chromite–olivine mineral pairs (18, 19) within five polished thin sections. The data are shown in Fig. 2, defining a tight trend parallel to the buffer curve defined by the stable coexistence of fayalite, magnetite, and quartz [the fayalite–magnetite–quartz oxygen buffer (FMQ)] but displaced to values ≈2.8 log units higher (i.e., FMQ+2.8). We interpret these data to result from local closed-system re-equilibration of each coexisting chromite–olivine pair as temperature dropped during solidification and cooling of the meimechites. The composition of the liquidus olivine (20) predicted for the aphyric sample 2 FG-50 ($Fo_{90.2}$) matches well to the measured compositions of the olivine crystals in the crystal-rich half of the same sample ($Fo_{90.8}$) and indicates a low-pressure olivine liquidus temperature of 1451°C and log fO_2 of FMQ+2.8.

A further check on the prevailing fO_2 during olivine crystallization was performed by analyzing vanadium in 10 melt inclusions hosted by olivine and inferred to represent melt trapped at equilibrium with the growing olivine crystals. The concentration of vanadium in the melt inclusions was determined by laser ablation ICP-MS (21) at Eidgenössische Technische Hochschule Zürich (Zürich, Switzerland). Ablation was carried out with a GeoLas 193-nm ArF Excimer laser (Lambda Physik, Göttingen, Germany) operated at 70- to 85-mJ output energy and employing a pulsed beam with an energy-homogenized beam profile (22). Ablated aerosols were transported by a He–Ar carrier gas mixture into an ELAN 6100 quadrupole ICP-MS (PerkinElmer, Wellesley, MA) operated in dual detector mode (23). Among other major and trace elements not reported here, the isotope ^{51}V was measured at a dwell time of 10 ms and settling time of 3 ms. The data reduction procedure (21, 24) used the reference glass SRM610 from the National Institute of Standards and Technology to calibrate analyte sensitivities and the concentration of Mg in the melt inclusions as the internal standard to calculate the absolute concentration of V in the melt phase. Some inclusions were opaque and interpreted to have been devitrified, but because the entire inclusion was ablated in each analysis, the signal could be integrated over the entire period of inclusion ablation. Ablation volumes were chosen so that the diameters of the spots illuminated by the laser were 10–15 μm larger than the diameters of the inclusions, which themselves were between 15 and 30 μm in diameter. We assumed a constant Mg concentration in the melt inclusions and calculated this constant Mg value by using the partitioning relationship for Fe and Mg (20) and the inclusion mass factor method (21). The ratio of V concentration in host olivine divided by that in the inclusion is taken as a measure of the partition coefficient $D_V^{ol/melt}$, which is known to be a sensitive function of fO_2 at which the olivine equilibrates with melt (25). The average of the 10 measured values of $D_V^{ol/melt}$ is 0.0091, with a standard deviation of 0.0013, yielding an estimated log fO_2 of FMQ+2.5, in good agreement with the estimate of FMQ+2.8 from olivine–spinel oxygen geobarometry.

Discussion

At temperatures below the anhydrous upper mantle solidus, spinel lherzolite typically contains sulfides such as pentlandite, pyrrhotite, and chalcopyrite, which form during cooling of mss, in addition to the major rock-forming silicate and oxide phases. Bockrath *et al.* (8) recently demonstrated that mss and sulfide

Table 1. Compositions of Siberian meimechites and alkali picrites

	Sample								
	2FG50								
Element	Phyric	Aphyric	G3345	2FG38	G3265	2FG40	2FG41	G49	Det limit
WXRF, wt % (glass bead)									
SiO_2	38.70	38.20	38.31	38.36	38.44	38.17	38.44	38.55	0.01
TiO_2	3.60	4.46	2.43	2.65	3.40	2.63	2.75	3.18	0.01
Al_2O_3	4.09	4.68	4.80	3.17	4.52	3.38	3.64	4.80	0.01
Fe_2O_3	14.98	15.96	12.54	13.75	14.40	14.15	13.45	13.61	0.01
MnO	0.21	0.22	0.17	0.20	0.20	0.20	0.20	0.20	0.01
MgO	22.70	19.42	29.89	27.87	23.33	27.93	27.94	24.25	0.01
CaO	7.25	8.70	5.08	5.93	7.96	5.72	5.89	6.68	0.01
Na_2O	0.19	0.19	0.21	0.17	0.32	0.15	0.16	0.18	0.01
K_2O	1.95	2.39	1.03	0.55	0.74	0.38	0.46	1.84	0.01
P_2O_5	0.45	0.59	0.36	0.34	0.48	0.35	0.37	0.41	0.01
LOI	5.39	4.82	4.78	7.00	6.42	7.76	7.71	4.99	0.05
ICP, ppm									
Rb	59.15	71.51	29.31	24.66	23.83	15.94	18.75	51.14	0.05
Sr	569.6	662.1	483.7	399.9	555.6	408.1	426.9	687.7	0.50
Y	17.54	21.93	12.05	13.16	17.55	13.15	13.73	15.63	0.02
Zr	321.8	404.1	203.7	226.3	281.1	226.0	234.8	283.3	4.00
Nb	69.3	>80	37.6	47.6	57.7	46.5	49.3	59.2	0.20
Hf	7.7	9.6	4.8	5.4	6.8	5.4	5.7	6.7	0.10
Ta	4.02	5.06	2.18	2.71	3.26	2.74	2.92	3.41	0.17
U	1.369	1.837	0.799	0.824	1.200	0.443	0.515	1.133	0.007
Th	5.49	7.00	2.98	3.75	4.59	3.78	4.00	4.66	0.06
La	60.72	77.05	33.11	41.77	51.00	42.76	45.00	52.62	0.02
Ce	131.5	168.0	73.87	90.15	110.6	93.04	96.87	114.8	0.07
Pr	15.98	20.42	9.329	11.03	13.53	11.39	11.93	14.04	0.006
Nd	62.86	80.11	37.86	44.12	54.41	45.47	46.37	55.32	0.03
Sm	10.46	13.26	6.80	7.59	9.61	7.72	8.01	9.22	0.01
Eu	2.935	3.693	1.924	2.130	2.728	2.166	2.244	2.568	0.005
Gd	7.323	9.157	4.893	5.330	6.893	5.355	5.642	6.390	0.009
Tb	0.914	1.159	0.611	0.673	0.879	0.675	0.719	0.797	0.003
Dy	4.449	5.595	3.067	3.230	4.388	3.303	3.491	3.968	0.008
Ho	0.714	0.911	0.481	0.524	0.706	0.534	0.558	0.636	0.003
Er	1.649	2.117	1.111	1.234	1.646	1.243	1.282	1.477	0.008
Tm	0.195	0.247	0.134	0.145	0.190	0.148	0.152	0.176	0.003
Yb	1.18	1.48	0.78	0.87	1.16	0.89	0.91	1.02	0.003
Lu	0.149	0.183	0.095	0.107	0.141	0.109	0.114	0.127	0.003
WXRF, ppm									
Co	114	96	123	116	104	114	117	119	12
Cr	1760	1456	2398	2226	1797	2068	2133	1947	4
Cu	171	203	91	119	119	117	118	132	1
Ni	1128	843	1585	1427	1174	1454	1430	1225	2
NFA, ppb									
Ir	1.37	1.06	1.57	2.02	1.58	1.72	1.86	1.51	0.04
Ru	2.28	2.03	3.24	2.90	2.29	2.86	2.59	2.46	0.13
Rh	0.46	0.36	0.44	0.52	0.47	0.46	0.43	0.46	0.08
Pt	7.76	9.05	5.91	7.90	11.14	7.03	7.12	6.94	0.14
Pd	3.90	3.19	4.46	4.33	7.26	3.55	3.86	3.25	0.11
Au	2.61	2.73	2.56	3.09	2.90	2.37	3.31	2.62	0.71

Analytical methods are presented in the text. WXRF, wavelength dispersive x-ray fluorescence.

liquid coexist over a wide range of temperatures at a given pressure at an fO_2 that lies somewhere below that at which graphite coexists with CO_2 (i.e., CCO buffer). Fig. 3 shows a portion of the system Fe–S–O at 1050°C and 1 atmosphere (26). At any given externally fixed fO_2 and sulfur fugacity (fS_2), there is only one possible sulfide melt composition. When sulfide and silicate melts are at equilibrium, the fO_2/fS_2 ratio is a function of the activity of FeO in the silicate melt (27, 28). Therefore, the coexistence of sulfide melt and silicate melt at a given fO_2 fixes fS_2. The solidus temperature and initial sulfide melt composition in a system containing spinel and mss are thus fixed by aFeO in the coexisting silicate melt and by fO_2. In Fig. 3, we show two melting paths followed by mss–magnetite mixtures with externally buffered fO_2, based on the gas fugacities plotted in ref. 26 and the assumption of fixed fO_2/fS_2 during melting. Both start at temperatures of <1050°C but above the mss–magnetite–wustite reaction point at 934°C (26). The FMQ-2 path begins at the magnetite–mss cotectic, and after a short period of cotectic

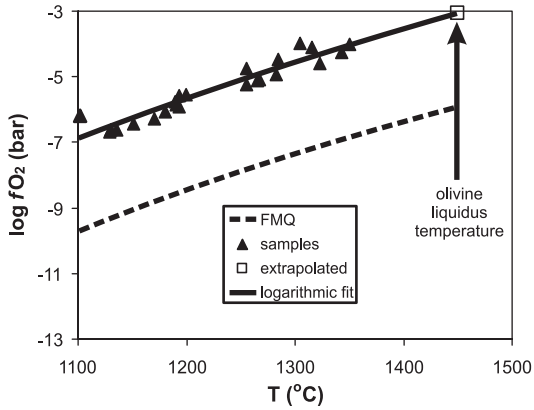

Fig. 2. Temperature and oxidation state of olivine–spinel pairs from Siberian meimechite samples. The solid line is a logarithmic best fit to the data, extrapolated to the liquidus temperature inferred by using Mg–Fe partitioning between olivine and melt.

melting all magnetite is consumed, leaving mss and sulfide liquid. This process is the situation reproduced by melting experiments at or below the CCO buffer (8). At FMQ, melting begins on the mss–magnetite cotectic at or just below 1050°C, but mss is consumed first, leaving only magnetite and liquid sulfide after only a very short interval of rising temperature.

The exact positions of the relevant phase boundaries under mantle conditions are not known, because they depend on pressure as well as the activities of FeS in Ni- and Cu-bearing mss and Fe_3O_4 in spinel. The effects of increasing pressure, decreasing Fe_3O_4 activity in spinel, and increasing proportion of NiS and CuS in the sulfide melt are to shift the spinel–mss cotectic toward the Fe–S join (29, 30). The arguments presented in this section are therefore qualitative rather than quantitative, but they are offered to illustrate a fundamental point: that at an indeterminate fO_2 higher than FMQ, the solid mantle assemblage mss+spinel should be expected to melt in the divariant field of spinel+sulfide melt, whereas at lower fO_2, melting will occur in the divariant field of mss+sulfide melt, regardless of the actual FeO content of the sulfide melt. In the former case, one expects to see complete melting of residual mss over a short temperature range, whereas in the latter case the mss and sulfide melt may coexist over a wide range of temperatures.

The iridium-group PGE (IPGE; Os, Ir, Ru, and Rh) are strongly partitioned into mss under fO_2 and fS_2 typical of coexisting silicate and sulfide melts whereas the platinum-group PGE (PPGE; Pt and Pd) and Au are excluded from mss and enter the sulfide melt (29). As a result, when silicate melt equilibrates with both mss and sulfide melt, the IPGE are much more strongly depleted than the PPGE, leading to a pronounced fractionation among the PGE. We therefore anticipate that partial melts of the upper mantle produced at moderate to low fO_2 should retain strongly fractionated PGE patterns until mss is completely melted out, whereas even small-degree partial melts produced at high fO_2 should have relatively unfractionated PGE patterns because of relatively early melting of mss to leave a spinel residue.

Oxidation of sulfide to sulfate is also critically important. At fO_2 exceeding FMQ+2, most sulfur dissolved in basaltic melt is present as SO_4^{-2} rather than S^{-2} (31). Based on experimental measurements of oxidation of sulfur as a function of fO_2 in basaltic melts (31), we estimate that ≈80% of the sulfur in our samples of meimechite and alkali picrite was oxidized, reducing the amount of sulfide available to participate in melting reactions to ≈50 ppm. Whereas the solubility of sulfide in silicate melts is on the order of 1,000 ppm (5), that of sulfate may be >1 wt% (32). We can account for the effects of high fO_2 in our melting models in either of two essentially equivalent ways. Either (*i*) the total amount of sulfur in the model mantle remains at 250 ppm but its solubility is increased to 1 wt%, or (*ii*) the amount of sulfur is reduced to 50 ppm but its solubility is kept at 1,000 ppm, to reflect the contribution only of sulfide to the mass balance.

In Fig. 4, we show the compositions of alkali picrite (this work), Hawaiian tholeiitic OIB (7), and normal MORB (7) along with the results of models incorporating the combined effects of mss and sulfide oxidation on the comportment of the chalcophile elements. Melting was modeled as a batch equilibrium process given a pyrolite mantle composition (6), reasonable partition coefficients for chalcophile elements between solid restite, silicate melt, mss, and sulfide liquid (33), and a degree of partial melting as input. S distribution between restite and silicate melt is calculated first from the stated solubility of S in the melt, and the amount left in restite is used to make mss or sulfide liquid with modal abundance of sulfide phases assumed to be 2.75 times the weight fraction of S. The relative proportions of solid restite, mss, and sulfide liquid are used to calculate a bulk partition coefficient to be used in the equilibrium melting equation $C_i^{\text{melt}} = C_i^{\text{bulk}}/((D(1 - F) + F)$ where C_i^{melt} and C_i^{bulk}

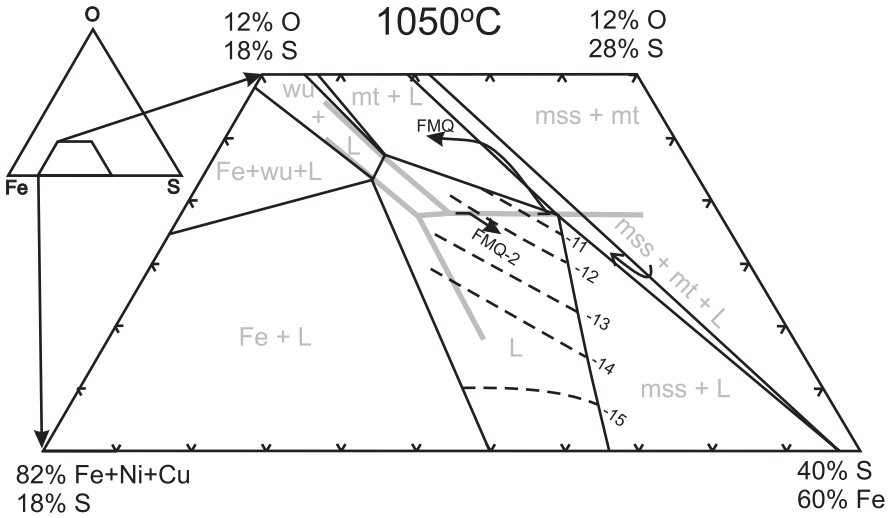

Fig. 3. Phase relations in the system Fe-S-O at 1050°C and 1 atm, with coordinates in wt% (26). Fields of liquid and solid stability are shown. Dashed lines represent fO_2 at equilibrium with sulfide liquids.

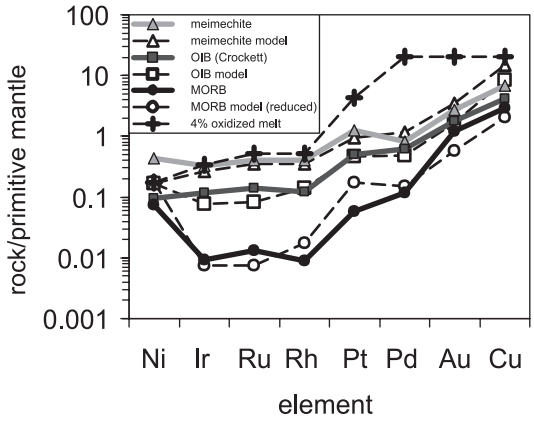

Fig. 4. Chalcophile element distributions during mantle melting. Shown are data for meimechite, OIB, and MORB along with model assumptions as described in the text.

are concentrations of an element in silicate melt and bulk mantle (i.e., restite+melt), respectively; D is the Nernst partition coefficient; and F is the wt fraction of melt in the system.

Because the relevant phase relations are known only approximately as functions of temperature, pressure, metal ratios, fO_2, and fS_2, we cannot predict exactly what proportions of mss and sulfide liquid will coexist with silicate melt in a given situation. Furthermore, the solidus temperature of the peridotite itself is a very sensitive function of the volatile content (34), which remains a poorly constrained parameter even in the best-studied suites of rocks. Although the dry peridotite solidus is above the mss liquidus at pressures of <3 GPa, the addition of only a fraction of a wt% of H_2O to dry peridotite will bring it well down into the divariant mss melting field (8, 34).

Reasonable choices of phase proportions yield satisfactory fits to the data (Fig. 4). For example, the Siberian alkali picrite data are reproduced by a model in which fO_2 is greater than FMQ+2, the sulfur solubility is 1.0 wt%, and, at 2.4% partial melting, the source peridotite retains only 6 ppm of S as sulfide melt.

The Hawaiian tholeiitic OIB is well fitted by a model of 2.3% partial melting at a sulfur solubility of 1.0 wt% if the restite contains 20 ppm of sulfide as an assemblage comprising 70% liquid and 30% mss, due to melting along the spinel–mss cotectic at an intermediate fO_2 near or slightly above FMQ. Because the OIB has equilibrated at a lower silicate/sulfide mass ratio, the overall PGE concentrations are lower; furthermore, the presence of mss causes a slight depletion in the IPGE relative to PPGE. The strongly fractionated, PGE-depleted signature of MORB can be accounted for by modeling 12% melting of a relatively reducing mantle below FMQ with sulfur solubility of 1,000 ppm in the silicate melt, containing 120 ppm of residual sulfide comprising 30% melt and 70% mss (35). The comparatively high modal proportion of residual sulfide containing abundant mss causes the extremely depleted and fractionated signature of the MORB magma.

At slightly higher degrees of partial melting at high fO_2, such as the oxidized 4% partial melt illustrated in Fig. 4, all sulfide is removed from the source mantle and the silicate melt contains abnormally high PPGE concentrations with Pt and Pd concentration of several tens of parts per billion. The concentrations of Os, Ir, Ru, Rh, and Pt might be controlled by the presence in the restite of alloy phases (36–38), but these phases do not sequester Pd or Au. Magmas with extreme Pd and Au contents have not hitherto been recognized in nature, but we point out that a globule of native Au containing ≈1.5% Pd, and inferred to have been present as a metal liquid, has been observed in OIB glass in Hawaii (39). The glass was not analyzed for PGE and Au, but the melt must have been exceedingly Au-rich to have been saturated with liquid Au (40).

Conclusions

The compositions of many moderate to small-degree partial melts of the upper mantle cannot be accounted for by using the canonical assumption that sulfide liquid in their source was not consumed until ≈25% partial melting. We show that models taking into account the combined effects of (*i*) divariant melting of mss in mantle fluxed by the addition of volatiles, and (*ii*) oxidation of sulfide to sulfate, can account for the observed compositions.

The results have several implications as follows.

1. Concentrations and relative fractionation of the chalcophile elements in magmas are extremely sensitive to oxidation state in the source mantle.
2. The strongly IPGE-depleted signatures of both oceanic and continental crust reflect mss fractionation at moderate fO_2 during the extraction of the crust from the mantle. Melt-depleted peridotite should be IPGE-enriched.
3. Oxidized alkaline picrites are very rich in PGE and Au. Economic concentrations of sulfide melt may form if assimilation of coal or hydrocarbons or crystallization of magnetite (41) causes reduction of some of their abundant sulfate to sulfide or if sulfur solubility is reduced by increasing silica activity during magma evolution or contamination. Hydrothermal deposits of Au and Pd may form directly from oxidized alkaline picrites in the absence of sulfide melt. The common association of PGE placer deposits with oxidized alkaline ultramafic Uralian–Alaskan type complexes (33) may reflect high PGE concentrations in their parental magmas.
4. The inference that the source of OIB was more oxidized than that of MORB may provide further evidence of the presence of a recycled component in the OIB source. The oxidized component may be oceanic crust that lost aqueous fluid during subduction. Alternately, it may have resulted from disproportionation of Fe^{2+} to liquid Fe metal and Fe^{3+} during crystallization of magnesium silicate perovskite in the lower mantle (42).

We thank Zoltán Zajacz for performing some of the laser ablation ICP-MS analyses of melt inclusions, Tony Naldrett for reading an earlier version of this manuscript and giving helpful comments, and J. P. Lorand and W. McDonough for formal reviews of this manuscript that prompted significant improvements in clarity. This work was supported by Natural Sciences and Engineering Research Council (Canada) Grant RGPIN 227836-04.

1. MacLean, W. H. (1969) *Econ. Geol.* **64,** 865–884.
2. Rehkämper, M., Halliday, A. N., Fitton, J. G., Lee, D.-C., Wieneke, M. & Arndt, N. T. (1999) *Geochim. Cosmochim. Acta* **63,** 3915–3934.
3. Lorand, J. P. (1993) *Earth Planet. Sci. Lett.* **119,** 627–634.
4. Peach, C. L., Mathez, E. A. & Keays, R. R. (1990) *Geochim. Cosmochim. Acta* **54,** 3379–3389.
5. Mavrogenes, J. A. & O'Neill, H. St. C. (1999) *Geochim. Cosmochim. Acta* **63,** 1173–1180.
6. McDonough, W. F. & Sun, S.-S. (1995) *Chem. Geol.* **120,** 223–253.
7. Crockett, J. H. (2002) in *The Geology, Geochemistry, Mineralogy and Beneficiation of PGE*, CIM Special Volume, ed. Cabri, L. J. (Can. Inst. of Mining, Metallurgy, and Petroleum, Montreal), Vol. 54, pp. 177–210.
8. Bockrath, C., Ballhaus, C. & Holzheid, A. (2004) *Science* **305,** 1951–1953.
9. Mungall, J. E. & Su, S. (2005) *Earth Planet. Sci. Lett.* **234,** 135–149.
10. Mungall, J. E. (2002) *Geology* **30,** 915–918.
11. Le Maitre, R. W., Bateman, P., Dudek, A., Keller, J., Lameyre, J., Le Bas, M. J., Sabine, P. A., Schmid, R., Sørensen, H., Streckeisen, A., *et al.* (1989) *Classification of Igneous Rocks and Glossary of Terms* (Blackwell, Oxford).
12. Arndt, N., Lehnert, K. & Vasil'ev, Y. (1995) *Lithos* **34,** 41–59.

13. Arndt, N. T., Chauvel, C., Fedorenko, V. & Czamanske, G. (1998) *Contrib. Mineral. Petrol.* **133,** 297–313.
14. Richardson, T. & Burnham, O. M. (2002) *Ont. Geol. Surv. Open File Rep.* **6100,** 35-1–35-5.
15. Meisel, T. & Moser, J. (2004) *Chem. Geol.* **208,** 319–338.
16. Griffin, W. L., Graham, S., O'Reilly, S. Y. & Pearson, N. J. (2004) *Chem. Geol.* **208,** 89–118.
17. Luguet, A., Lorand, J. P. & Seyler, M. (2003) *Geochim. Cosmochim. Acta* **67,** 1553–1570.
18. O'Neill, H. St. C. & Wall, V. J. (1987) *J. Petrol.* **28,** 1169–1191.
19. Ballhaus, C., Berry, R. F. & Green, R. H. (1990) *Nature* **348,** 437–440.
20. Roeder, P. L. & Emslie, R. F. (1970) *Contrib. Mineral. Petrol.* **29,** 275–289.
21. Halter, W. E., Pettke, T., Heinrich, C. A. & Rothen-Rutishauser, B. (2002) *Chem. Geol.* **183,** 63–86.
22. Gunther, D., Frischknecht, R., Muschenborn, H. J. & Heinrich, C. A. (1997) *Fresenius' J. Anal. Chem.* **359,** 390–393.
23. Pettke, T., Heinrich, C. A., Ciocan, A. C. & Gunther, D. (2004) *J. Anal. Atom. Spectrom.* **15,** 1149–1155.
24. Longerich, H. P., Jackson, S. E. & Gunther D. (1996) *J. Anal. Atom. Spectrom.* **11,** 899–904.
25. Canil, D. & Fedortchouk, Y. (2001) *Can. Mineral.* **39,** 319–330.
26. Naldrett, A. J. (1969) *J. Petrol.* **10,** 171–202.
27. Wallace, P. & Carmichael, I. S. E. (1992) *Geochim. Cosmochim. Acta* **56,** 1863–1874.
28. O'Neill, H. St. C. & Mavrogenes, J. A. (2002) *J. Petrol.* **43,** 1049–1087.
29. Mungall, J. E., Andrews, D. R. A., Cabri, L. J., Sylvester, P. J. & Tubrett, M. (2005) *Geochim. Cosmochim. Acta* **69,** 4349–4360.
30. Urakawa, S., Kato, M. & Kumazawa, M. (1987) in *High-Pressure Research in Mineral Physics*, eds. Mangnani, M. H. & Syono, Y. (Am. Geophys. Union, Washington, DC), pp. 95–111.
31. Jugo, P. J., Luth, R. W. & Richards, J. P. (2005) *Geochim. Cosmochim. Acta* **69,** 497–503.
32. Jugo, P. J., Luth, R. W. & Richards, J. P. (2005) *J. Petrol.* **46,** 783–798.
33. Mungall, J. E., ed. (2005) *Exploration for Platinum-Group Element Deposits*, Mineralogy Association of Canada Short Course (Miner. Assoc. of Can., Quebec), Vol. 35, pp. 1–34.
34. Katz, R. F., Spiegelman, M. & Langmuir, C. H. (2003) *Geochem. Geophys. Geosyst.* **4,** 10.1029/2002GC000433.
35. Bezos, A., Lorand, J.-P., Humler, E. & Gros, M. (2005) *Geochim. Cosmochim. Acta* **69,** 2613–2627.
36. Borisov, A. & Palme, H. (2000) *Am. Mineral.* **85,** 1665–1673.
37. Peck, D. C., Keays, R. R. & Ford, R. J. (1992) *Aust. J. Earth Sci.* **39,** 373–387.
38. Brenan, J. M. & Andrews, D. (2001) *Can. Mineral.* **39,** 341–360.
39. Sisson, T. W. (2003) *Econ. Geol.* **98,** 643–648.
40. Hanley, J. J., Pettke, T., Mungall, J. E. & Spooner, E. T. C. (2005) *Geochim. Cosmochim. Acta* **69,** 2593–2611.
41. Sun, W., Arculus, R. J., Kamenetsky, V. S. & Binns, R. A. (2004) *Nature* **431,** 975–978.
42. Wade, J. & Wood, B. J. (2005) *Earth Planet. Sci. Lett.* **236,** 78–95.